Differential response of MDA-MB-231 breast cancer and MCF10A normal breast cells to cytoskeletal disruption

SANGWOO KWON[1], SE JIK HAN[1,2] and KYUNG SOOK KIM[1]

[1]Department of Biomedical Engineering, College of Medicine, and [2]Department of Biomedical Engineering, Graduate School, Kyung Hee University, Seoul 02447, Republic of Korea

Received March 31, 2023; Accepted July 27, 2023

DOI: 10.3892/or.2023.8637

Abstract. Metastasis remains a major clinical problem in cancer diagnosis and treatment. Metastasis is the leading cause of cancer-related mortality but is still poorly understood. Cytoskeletal proteins are considered potential therapeutic targets for metastatic cancer cells because the cytoskeleton serves a key role in the migration and invasion of these cells. Vimentin and F-actin exhibit several functional similarities and undergo quantitative and structural changes during carcinogenesis. The present study investigated the effects of vimentin and F-actin deficiency on the survival and motility of breast cancer cells. In metastatic breast cancer cells (MDA-MB-231) and breast epithelial cells (MCF10A), vimentin was knocked down by small interfering RNA and F-actin was depolymerized by latrunculin A, respectively. The effect of reduced vimentin and F-actin content on cell viability was analyzed using the MTT assay and the proliferative capacity was compared by analyzing the recovery rate. The effect on motility was analyzed based on two processes: The distance traveled by tracking the cell nucleus and the movement of the protrusions. The effects on cell elasticity were measured using atomic force microscopy. Separately reducing vimentin or F-actin did not effectively inhibit the growth and motility of MDA-MB-231 cells; however, when both vimentin and F-actin were simultaneously deficient, MDA-MB-231 cells growth and migration were severely impaired. Vimentin deficiency in MDA-MB-231 cells was compensated by an increase in F-actin polymerization, but no complementary action of vimentin on the decrease in F-actin was observed. In MCF10A cells, no complementary interaction was observed for both vimentin and F-actin.

Correspondence to: Professor Kyung Sook Kim, Department of Biomedical Engineering, College of Medicine, Kyung Hee University, 26 Kyungheedae-ro, Dongdaemun, Seoul 02447, Republic of Korea
E-mail: moosou94@khu.ac.kr

Key words: vimentin, F-actin, metastatic cancer, breast cancer, targeted therapy

Introduction

The cytoskeleton is a dynamic network of filamentous proteins that controls cell shape, maintains intracellular organization and is involved in cell motility (1,2). Alterations in cytoskeletal structures serve a pivotal role in controlling cancer cell behavior, including cell adhesion, migration and invasion (3,4).

The cytoskeleton comprises three proteins: Actin filaments (F-actin), intermediate filaments, microtubules and various filament-associated proteins such as molecular motors (2). Among the protein filaments, vimentin and F-actin undergo pronounced changes during tumorigenesis. Vimentin, a type III intermediate filament, is highly expressed in mesenchymal cells compared with that in epithelial cancer cells. In addition, vimentin expression is upregulated during the epithelial-mesenchymal transition (EMT) (5,6). Cancer cells lose their junctions during EMT and undergo morphological changes from epithelial cells with an apical-basal polarity to a spindle-shaped mesenchymal phenotype (7). Overexpression of vimentin in cancer cells is correlated with tumor growth, metastasis and poor prognosis (8,9).

Unlike vimentin, F-actin is downregulated in most cancer cells. Therefore, the relative content of F-actin to vimentin in cancer cells is lower than in normal cells (10). In normal cells, F-actin content is higher than vimentin. F-actin has a highly dynamic structure that undergoes continuous polymerization and degradation. A monomer of actin (G-actin) polymerizes to F-actin under physiological conditions and F-actin dissociates to G-actin to maintain equilibrium (11). Dynamic organization of F-actin is a prerequisite for cancer cell migration and invasion. Reduced F-actin results in changes in the mechanical properties of cancer cells; specifically, cancer cells are less elastic than normal cells (10).

Cytoskeletal proteins are emerging as attractive therapeutic targets for inhibiting cancer metastasis because they serve important roles in cancer cell migration and invasion. Several compounds, such as ajoene, ginsenosides, withaferin A (WFA) and arylquin 1 have been introduced as vimentin-targeting drugs (12). They downregulate vimentin expression, induce disassembly of vimentin filaments and induce apoptosis. Dynamic actin assembly can be disrupted by pharmacological inhibitors, such as latrunculin A (LatA) and cytochalasin, which inhibit cancer cell migration and invasion (13,14). LatA blocks the new F-actin by sequestering G-actin, whereas

cytochalasin blocks the fast-growing barbed ends of F-actin. The disassembly and rearrangement of the F-actin can also be inhibited by these drugs. Pharmacologically perturbing the motility of cancer cells by altering vimentin and F-actin can alter their organotropism for growth and metastasis (15).

Therefore, compounds targeting cytoskeletal dynamics are of increasing interest in cancer therapeutics (16,17). However, only a handful of drugs have been proven effective and are in clinical trials and even those need further validation. For example, recent phase I safety and pharmacokinetic trials of WFA have confirmed the importance of using the minimum effective dose due to potential side effects (18,19). In the case of arylquin 1, it has been demonstrated that apoptosis can be induced in cancer cells by regulating the activity of Par-4 function, but additional analysis of the molecular mechanism is required (20,21). In addition, the clinical application of cytoskeleton-targeted therapeutics remains limited owing to several challenges. First, because of their ubiquitous role, cytoskeleton-targeted drugs can affect various processes in cancer and normal cells, including cell migration, proliferation and exocytosis (22). Second, it is challenging to sustain or irreversibly interrupt F-actin assembly. F-actin can be disassembled by drugs or external stress but rapidly reassembles and reorganizes to maintain homeostasis (23). Third, the importance of vimentin in metastasis has made it an attractive drug target; however, no drugs that specifically target intermediate filaments are currently in use (24). However, more specific vimentin-targeting drugs with low toxicity are still needed. Fourth, the complementary actions of F-actin and vimentin in response to forced inhibition are poorly understood. As vimentin and F-actin have similar mechanisms of action, particularly in cell motility and structure formation, it is important to understand the relationship and interactions between the two proteins.

To overcome the shortcomings of the current cytoskeleton-targeting drugs and develop effective cancer therapeutics via cytoskeletal protein modulation, the present study investigated the effects of vimentin and actin deficiency on metastatic cancer cells. It is well known that the content of F-actin is reduced, and that of vimentin is increased, in cancer cells compared with normal cells. Therefore, the present study focused on the complementary interactions between vimentin and F-actin. Vimentin and F-actin levels were reduced by ~50% in both cancer (MDA-MB-231) and normal (MCF10A) cells. The effect of F-actin downregulation on vimentin expression in cancer and normal cells was analyzed. Changes in F-actin levels caused by vimentin reduction were also analyzed as were the effects of altering the expression of vimentin and F-actin on cell viability, morphology and motility.

Materials and methods

Cell culture. The metastatic breast cancer cell line (MDA-MB-231) was purchased from the Korean Cell Line Bank (KCLB; Seoul, Korea) and cultured in Roswell Park Memorial Institute (RPMI) 1640 medium (Thermo Fisher Scientific, Inc.) with 10% fetal bovine serum (Gibco; Thermo Fisher Scientific, Inc.), 1% antibiotics/antimycotics, 300 mg/l L-glutamine, 25 mM hydroxyethyl piperazine ethanesulfonic acid and 25 mM sodium bicarbonate. Normal epithelial cells (MCF10A) were purchased from the American Type Culture Collection. MCF10A cells were cultured using Dulbecco's modified Eagle's medium/nutrient mixture F-12 (DMEM/F-12) (Thermo Fisher Scientific, Inc.) with 5% horse serum, 20 ng/ml epidermal growth factor (EGF), 0.5 mg/ml hydrocortisone, 100 ng/ml cholera toxin, 10 μg/ml insulin and 1% antibiotics/antimycotics.

Cell viability. Cell viability was analyzed using a 3-(4,5-dimethylthiazol-2-yl)-2,5-diphenyl tetrazolium bromide (MilliporeSigma) assay to determine the effects of vimentin knockdown and F-actin depolymerization. MCF10A and MDA-MB-231 cells were seeded into 35-mm diameter culture dishes at a density of $4.5x10^5$ cells/well. After two days of small interfering (si) RNA transfection and 2 min of LatA treatment, the cells were incubated for 12 and 24 h. EZ-Cytox solution (DoGen Bio, Seoul, Korea) was added to each cell dish (10 ml) and incubated at 37˚C for 1 h. A Multiskan EX ELISA microplate reader (Thermo Fisher Scientific, Inc.) was used to measure the absorbance at 450 nm.

siRNA knockdown of vimentin. Cells were seeded at ~70% confluence for siRNA transfection and cultured for 24 h. For MDA-MB-231 cells, transfection reagents Opti-MEM I (300 μl; Thermo Fisher Scientific, Inc.), Lipofectamine (9 μl; Invitrogen; Thermo Fisher Scientific, Inc.) and 21-mer siRNA (Thermo Fisher Scientific, Inc.; cat. no. 4390824; 5 μl) were used. The sequence of siRNA is 5' GGUUGAUACCCACUC AAAATT-3' and 3'-TTAAAACUCACCCAUCGUUGG-5'. For MCF10A cell transfection, 20 μl of siRNA was added. The negative control (NC) siRNA (Thermo Fisher Scientific, Inc.; cat. no. 4390843; 3 μl) was added to Opti-MEM (300 μl) and Lipofectamine (9 μl). After 5 min of incubation at room temperature, transfection solutions were added to the cells. After two days of incubation, the transfected cells were visualized by fluorescence microscopy and analyzed by western blotting.

F-actin depolymerization. Cells were seeded at a density of $0.5x10^5$ cells/well in 35-mm diameter culture dishes. MDA-MB-231 cells were treated with LatA (Invitrogen; Thermo Fisher Scientific, Inc.) at a concentration of 0.3 μM for 2 min (37˚C) to depolymerize the F-actin content to ~50%. MCF10A cells were treated with LatA at a concentration of 0.5 μM for 2 min (37˚C). After 2 min of LatA treatment, the medium was replaced with fresh medium at 37˚C.

Analysis of cell recovery. To assess the effect of F-actin and vimentin deletion on cell growth, the present study compared how much the cells grew over time after actin and vimentin loss. Cell viability was measured by MTT assay at 0, 24 and 48 h following LatA treatment and siRNA knockdown of vimentin, respectively. To quantitatively analyze the effect of vimentin knockdown, cell viability after 24 and 48 h of siRNA transfection was normalized to the viability day zero. The values were then divided by the viability of the (NC) group and referred to as the recovery rate. Non-targeting siRNA was used as a NC to provide a baseline for target gene silencing by controlling for non-specific effects associated with siRNA

delivery. The untreated cells were designated as the positive-control (PC). The recovery rate is defined as follows:

$$Recovery\ rate = \frac{Via'_{1(2)}(siVim) - Via'_0(siVim)}{Via_{1(2)}(NC) - Via_0(NC)} \quad (1)$$

$$Recovery\ rate = \frac{Via'_{1(2)}(LatA) - Via'_0(LatA)}{Via_{1(2)}(PC) - Via_0(PC)} \quad (2)$$

$$Recovery\ rate = \frac{Via'_{1(2)}(Combined) - Via'_0(Combined)}{Via_{1(2)}(NC) - Via_0(NC)} \quad (3)$$

where $Via_{1(2)}(NC)$ and $Via_{1(2)}(PC)$ are the cell viability of the NC and PC groups after one (or two days) of culture, respectively. $Via_0^{'}(siVim)$ is the cell viability of transfected cells on day 1 of culture and $Via^{'}_{1(2)}(siVim)$ is the viability after 1 (or 2) days of culture. $Via^{'}_0(LatA)$ is the cell viability of LatA-treated cells on day 0 of culture and $Via^{'}_{1(2)}(siVim)$ is the viability after 1 (or 2) days of LatA treatment. $Via^{'}_0(Combined)$ is the viability of cells simultaneously depleted of vimentin and F-actin on day 0 of culture and $Via^{'}_{1(2)}(siVim)$ is the viability 1 (or 2) days after the depletion.

Western blotting. Cells were washed several times with phosphate-buffered saline (PBS) and scraped into a radioimmunoprecipitation assay buffer (Thermo Fisher Scientific, Inc.) containing a protease inhibitor cocktail. To separate intracellular proteins (vimentin and F-actin) and cell debris, the cells were centrifuged at 374 x g for 5 min at 4˚C. The supernatant was centrifuged at 15,000 x g for 5 min (4˚C) to separate F-actin in the form of pellets and the remaining solution contained G-actin. For determination of total protein concentration in each sample was used BCA Protein Assay Kit (Pierce; Thermo Fisher Scientific, Inc.). After protein quantification each sample (50 μg of protein) was prepared for SDS-PAGE by heating it in 5XSDS-PAGE loading buffer for 5 min at 95˚C. For western blot analysis, vimentin (10 μl), G-actin and F-actin proteins were separately loaded onto 12.5% polyacrylamide gels. The resolved proteins were transferred onto nitrocellulose membranes. The membrane was blocked with 5% fat-free milk in PBS (pH 7.4) for 30 min at room temperature and then incubated with primary anti-vimentin (Cell Signaling Technology Inc.; cat. no. 5741) or anti-actin (Cytoskeleton Inc.). Anti-vimentin and anti-actin antibodies were mixed with Tris-buffered saline with 0.01% Tween 20 (TBS-T) at 1:1,000 and 1:500 dilution, respectively, overnight at 4˚C. Finally, the membranes were treated with anti-rabbit secondary antibodies (GenDEPOT Inc.; cat. no. SA202-500)/fat-free milk at 1:6,500 dilution and incubated for 1 h at room temperature. Integrin was analyzed using a similar process as follows. The lysates were incubated for 30 min at 4˚C and then centrifuged at 14,207 x g for 20 min (4˚C). The supernatant was mixed with an equal amount of loading buffer (2XLaemmli sample buffer with 5% β-mercaptoethanol) and boiled for 5 min. The size marker (6 μl) and protein (40 μl) were separately loaded in 8.0% polyacrylamide gels. The resolved proteins were transferred to nitrocellulose membranes, blocked with 5% BSA/TBS-T for 1 h at room temperature and then incubated with a primary antibody [anti-integrin β1 antibody (P5D2); Abcam; cat. no. ab24693] at a 1:1,000 dilution overnight at 4˚C. The secondary antibody [Alexa Fluor 555 goat anti-mouse IgG (H+L); Abcam; cat. no. ab150114] was incubated with blocking buffer at a 1:5,000 dilution for 1 h at room temperature. Finally, the membranes were subjected to enhanced chemiluminescence (Pierce; Thermo Fisher Scientific, Inc.) and autoradiography using the ChemiDoc XRS+Imaging System (Bio-Rad Laboratories, Inc.).

Atomic force microscopy (AFM) and force distance (FD) curve measurement. The morphology and cellular elasticity were measured using AFM (Nano N8 Neos; Bruker Corporation) under liquid conditions. An Au-coated contact-mode probe (ContGD; BudgetSensors; Innovative Solutions Bulgaria Ltd.) was used for imaging and FD curve measurements. The detailed information of the contact mode probe was: Resonance frequency of 13 kHz (± 4 kHz), force constant of 0.2 N/m (0.07-0.4 N/m), cantilever length of 450 μm (± 10 μm), cantilever width of 50 μm (± 5 μm), cantilever thickness of 2 μm (± 1 μm), tip height of 17 μm (± 2 μm) and tip radius of <10 nm. The loading force and loading rate of the probe were set to <10 nN and <1 μm/s, respectively. FD-curve was analyzed using the Sneddon model (25).

Two-dimensional (2D) optical tracking assay. Cell migration in 2D was tracked in real-time at a low cell density of $0.5x10^5$ cells. Without fluorescent staining, the cells were placed in a portable incubator and the movement of the cells was measured at 1-min intervals for 4 h based on the position of the nucleus under an optical microscope (magnification, x20). The migration distance of a single cell was analyzed as a scalar value by using a video analysis and modeling program (Tracker, Video Analysis and Modeling Tool ver. 5.0.2; https://physlets.org/tracker/).

Analysis of protrusion dynamics. Single-cell movements were captured in real-time at 10 sec intervals for 30 min. Based on the change in light contrast in the optical image, the periodic motion of the protrusions on the leading edge of the cells was analyzed. Light contrast ranged from 0 luma (black) to 250 luma (white). The period and amplitude of the periodic function were extracted using an analysis program (Tracker, Video Analysis and Modeling Tool ver. 5.0.2; https://physlets.org/tracker/).

Immunofluorescence staining. Cells were fixed with 3.7% formaldehyde for 15 min at room temperature and then washed with PBS for 30 sec. Cells were treated with rhodamine-phalloidin (100 nM; Alexa Fluor 488 phalloidin; Invitrogen; Thermo Fisher Scientific, Inc.; cat. no. A12379) for F-actin fluorescence staining for 30 min at room temperature, washed several times with PBS and then stored in the dark at 4˚C. For vimentin fluorescence staining, cells were permeabilized in 0.5% TritonX/PBS for 5 min and blocked with bovine serum albumin (BSA; GenDEPOT Inc.) for 30 min at 21˚C. Cells were then incubated with primary antibodies [Vimentin (D21H3) XP Rabbit mAb, 1:200, Cell Signaling Technology Inc.; cat. no. 5741] for 1 h at 21˚C. A secondary antibody of Alexa Fluor 555 goat anti-rabbit IgG (H+L; Invitrogen; Thermo Fisher Scientific, Inc.; cat. no. SA202-500) was used at a 1:500 dilution for 1 h at 21˚C. A fluorescence optical microscope (Nikon Ti-E; Nikon Corporation) was used to detect rhodamine-phalloidin

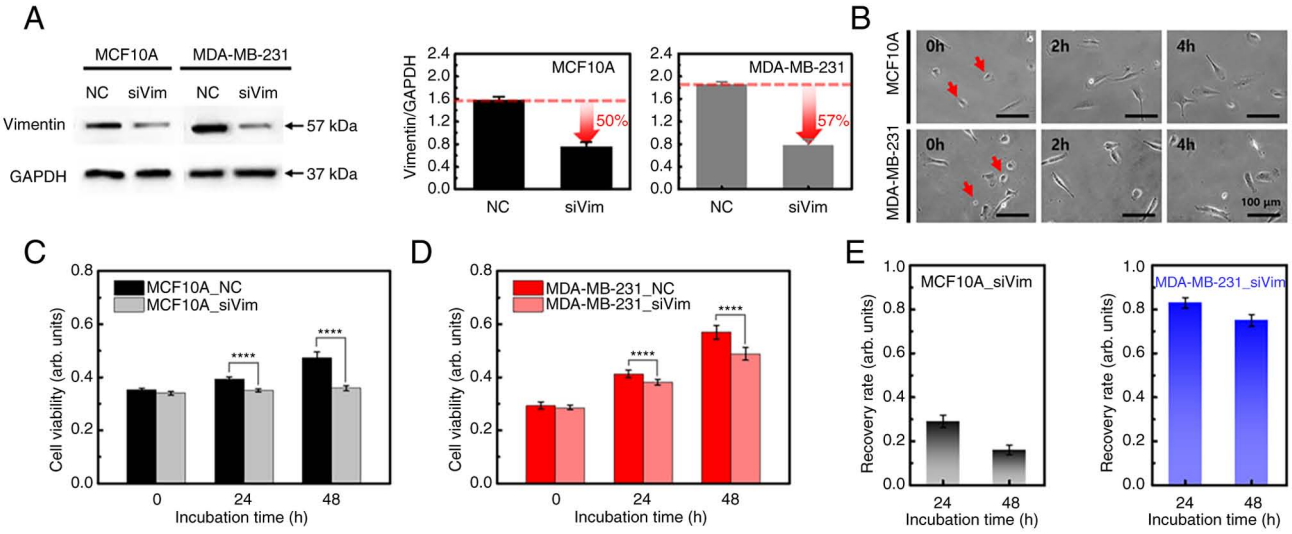

Figure 1. Effects of vimentin knockdown on cell viability and recovery rate. (A) Western blotting analysis of vimentin. Compared with control cells, vimentin expression levels were reduced by 50% in MCF10A and 57% in MDA-MB-231 cells. (B) Optical microscopic images of both cells were obtained after siRNA transfection for 4 h. Red arrows indicate contracted cells due to vimentin deficiency. Comparison of cell viability between the NC and siRNA-transfected of (C) MCF10A and (D) MDA-MB-231 cells. (E) The recovery rate of cell viability in MCF10A and MDA-MB-231 cells after 24 and 48 h of siRNA transfection. The recovery rate of MCF10A and MDA-MB-231 cells was calculated from the cell viability of (C) and (D), receptively. Error bars indicate the mean ± SD (t-test) of triplicate samples. ****P<0.0001 vs. NC. si, small interfering; NC, negative control.

(excitation: ~495 nm; emission: ~518 nm) and Alexa Fluor 555 (excitation: ~555 nm; emission: ~565 nm).

Statistical analysis. All data were statistically analyzed and expressed as mean ± standard deviation (SD). Analyses were performed using one-way ANOVA and post hoc analysis of Tukey's test. The software used for the statistical analysis was R program (2020-year; version 4.0.0; http://www.R-project.org/). P<0.05 was considered to indicate a statistically significant difference.

Results

Knockdown of vimentin differentially affects the growth of normal and cancer cells. Vimentin is a major intermediate filament protein that serves an essential role in the stabilization of cellular structures and migration. For vimentin knockdown, MCF10A and MDA-MB-231 cells were transfected with siRNA for two days. Western blotting confirmed partial knockdown of vimentin expression in both cell lines (Figs. 1A and S1). Non-targeting siRNA was used as NC group to provide a baseline for target gene silencing by controlling for the non-specific effects associated with siRNA delivery. Vimentin expression in siRNA-transfected (siVim) MCF10A cells was reduced by ~50% compared with that in the NC group. In MDA-MB-231 cells, vimentin expression was decreased by ~57% following siRNA transfection.

The two cell types contracted slightly immediately following vimentin deficiency. However, there was no significant change in adhesion to the matrix after 4 h (Fig. 1B). To investigate whether the loss of vimentin affects cell viability or proliferation, siVim cells were cultured for two days and their viability was compared with that of the NC group. Vimentin knockdown reduced the viability of both cell lines (Fig. 1C and D). There was no significant difference in cell viability after one day of transfection in either cell type; however, the difference increased over time. The viability of the NC group increased over time in MCF10A cells, whereas the siVim group showed no significant change (Fig. 1C). The viability of MDA-MB-231 cells increased over time in both NC and siVim groups (Fig. 1D). The difference in cell viability between the NC and siVim groups was statistically significant after 24 h for both MCF10A and MDA-MB-231 cells. These results demonstrated that vimentin serves a role in cell survival.

To quantitatively analyze the effect of vimentin knockdown, cell viability after one and two days of siRNA transfection was normalized to the viability on day zero. For MCF10A cells, the recovery rate was 29 and 16% after 1 and 2 days, respectively. In MDA-MB-231 cells, the recovery rate reached 83% on the 1st day of transfection and decreased slightly on the 2nd day (75%; Fig. 1E). These results indicated that the proliferation of MCF10A cells was significantly inhibited by vimentin deficiency, whereas the growth of MDA-MB-231 cells recovered over time.

Rearrangement and content change of F-actin to compensate for vimentin deficiency. Since F-actin serves an important role in the growth and migration of cancer cells, together with vimentin, the effect of vimentin deficiency on the distribution and content of F-actin was analyzed. In MCF10A cells, there were no notable changes in the cell shape or F-actin distribution due to vimentin deficiency (Fig. 2A). By contrast, cells exhibited rounded membrane edges were frequently observed in MDA-MB-231_siVim cells (Fig. 2B). Vimentin was mostly concentrated around the nucleus and F-actin was widely distributed in MDA-MB-231_siVim membranes.

Vimentin knockdown decreased the cell size by 24.5% in MCF10A cells and increased the cell size by 14.4% in MDA-MB-231 cells (Fig. 2C). MCF10A and MDA-MB-231

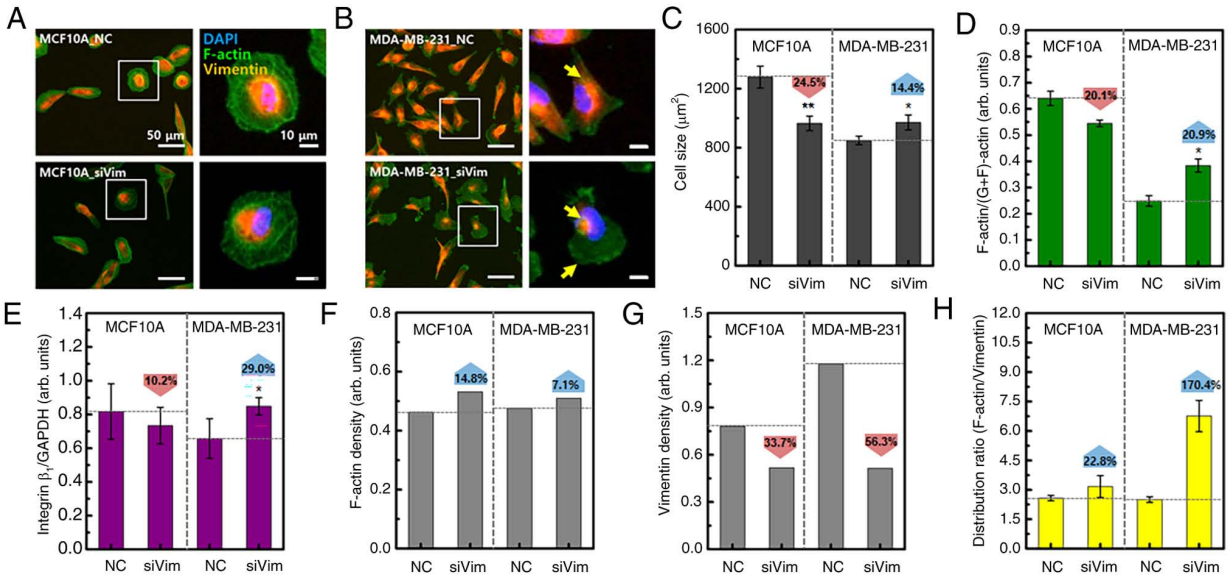

Figure 2. Effects of vimentin knockdown on cytoskeletal and adhesion proteins. Immunofluorescence staining of vimentin and F-actin in (A) MCF10A and (B) MDA-MB-231 cells. Yellow arrows indicate the distribution area of vimentin. Changes in the (C) cell size and contents of (D) F-actin and (E) integrin β1 by siRNA transfection were compared with NC. (F) The amount of F-actin in (D) divided by the cell size in (C) to obtain the F-actin density. (G) The amount of vimentin in (A) divided by the cell size in (C) to obtain the F-actin density. (H) The distribution ratio of F-actin and vimentin was calculated from the fluorescence images shown in (A) and (B). Error bars indicate the mean ± SD (t-test) of triplicate samples. si, small interfering; NC, negative control. *P<0.05; **P<0.01 vs. NC.

cells also showed differences in the content changes of F-actin and integrin β_1. F-actin and integrin β_1 are directly correlated with respect to adhesion to substrates required for cell migration. One side of the integrin attaches to the ECM forming focal adhesions and the other side connects to F-actin. As cells migrate, integrins repeatedly bind to and dissociate from the ECM. Depletion of integrin β_1 induces disruption of focal adhesions, resulting in inhibition of cell migration (26). For this reason, a quantitative experiment on integrin was performed. Vimentin knockdown reduced the levels of F-actin and integrin β_1 in MCF10A cells and increased their levels in MDA-MB-231 cells (Figs. 2D and E and S2). Consequently, the F-actin content relative to cell size increased after vimentin knockdown in both cell types (Fig. 2F). Compared with cell size, the vimentin content was reduced by 33.7% in MCF10A cells and 56.3% in MDA-MB-231 cells (Fig. 2G). As the average F-actin or vimentin content of the entire group was normalized to the average cell size, statistical significance was not analyzed (Fig. 2F and G). After vimentin knockdown, the intracellular distribution range of F-actin in MCF10A cells increased by 22.8 and 170.4% in MDA-MB-231 cells, compared with the vimentin distribution area (Fig. 2H). These results showed that the response to vimentin deficiency was different in MCF10A and MDA-MB-231 cell models. Normal cells appear to reduce in size to minimize the changes in cytoskeletal proteins caused by vimentin knockdown. By contrast, cancer cells appear to have an increased F-actin content to compensate for vimentin deficiency.

Vimentin knockdown affects cellular elasticity and motility. High-resolution AFM images were obtained for both MCF10A and MDA-MB-231 cells to obtain the FD-curve under liquid conditions. The image on the left in Fig. 3A depicts the topography of the MDA-MB-231 cells and the image on the right shows the error image of the topography. The error image is the output of the differential amplifier, which is measured by tracking the probe on the surface using optimal proportional-integral-differential (PID) parameters. Instantaneous phase differences appear where the height of the sample changes, allowing the nucleus and the cell body to be more clearly distinguished. The error image is, therefore, helpful in determining where to measure the FD-curve. The FD-curve was obtained from the body parts of the cells to avoid the influence of the nucleus and matrix. The measurement location of the FD curve was determined from the error image. FD-curve was obtained at 10 different locations on each cell and ~20 different cells in each group were measured.

The FD-curve for individual cells were extracted using the magnitude of the load applied to the cell based on the indentation depth of the AFM tip. The indentation depth was ~1,000 nm at a loading force of 5 nN. The FD-curve was analyzed using the Sneddon model because a pyramid-shaped tip was used for the measurements (27). Fig. 3B shows representative FD-curve obtained from MCF10A_NC and MCF10A_siVim cells. The slope of the FD-curve for MCF10A_siVim was larger than that for MCF10A_NC. A large slope indicated high elasticity. By contrast, the slope of the curve for the MDA-MB-231 cells decreased after siRNA transfection (Fig. 3C). The Young's modulus of MCF10A_NC (15.4±2.1 kPa) was higher than that of MDA-MB-231_NC (12.6±2.9 kPa; Fig. 3D and E). Notably, after vimentin knockdown, the elasticity was significantly increased in MCF10A_siVim (30.0±4.1 kPa) but decreased in MDA-MB-231_siVim (8.1±1.4 kPa). Opposite changes in Young's modulus were observed with a decrease in F-actin.

Since vimentin is a cytoskeletal protein involved in cell motility, the effect of vimentin loss on cell migration was investigated. In MCF10A_NC cells, the leading edge of the cell developed in one direction and the cell exhibited

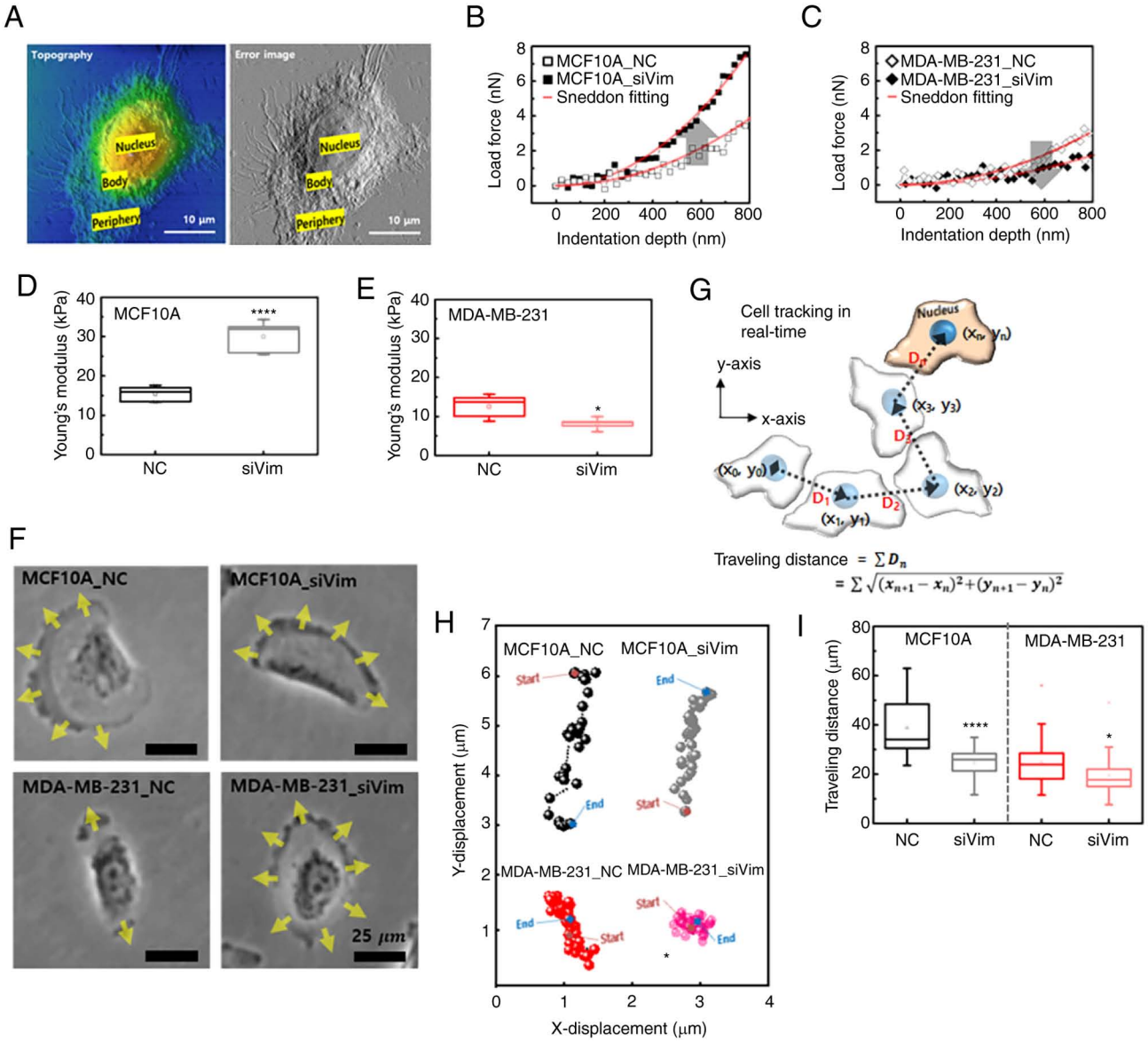

Figure 3. Mechanical property changes due to vimentin knockdown. (A) Representative AFM topography and error images of cells. The nucleus, body and periphery sites are marked in different colors. Representative force-distance curve obtained in (B) MCF10A and (C) MDA-MB-231 cells. Approach curve was fitted with the Sneddon model. Young's modulus of (D) MCF10A and (E) MDA-MB-231 cells was determined. (F) Comparison of cell movement before and after siRNA transfection. Arrows indicate protrusion. (G) Schematic diagram of a single-cell tracking system using an optical microscope. Cell migration was tracked in a Cartesian coordinate based on nuclear location at 1-min intervals for 4 h. (H) Cell displacement was converted to a scalar quantity. (I) Comparison of traveling distance before and after siRNA transfection. Error bars indicate the mean ± SD (t-test). *P<0.05; ****P<0.0001 compared with NC. AFM, atomic force microscopy; si, small interfering; NC, negative control.

directional movement (Fig. 3F; Video S1). There were no significant changes in the motility of MCF10A cells following vimentin deficiency. In MDA-MB-231_NC cells, the leading edge developed uniaxially; therefore, the cell did not move in one direction. Following vimentin deficiency, the leading edge developed in all directions, making directional movements more difficult (Fig. 3F). Cell movement was tracked in 2D space and traveling path was measured by scalar values (x_i, y_i) at 1.0 min intervals based on the nucleus (Fig. 3G). The directional movement of MCF10A cells was clearly visible in the traveling path observed for 4 h. MCF10A_NC and MCF10A_siVim cells both migrated mainly in the y-direction, as shown in Fig. 3H. MDA-MB-231 cells did not move in a specific direction and hovered at the same location. As expected, the total migration distance of the MCF10A cells was greater than that of the MDA-MB-231 cells (Fig. 3I). The MCF10A_NC migrated 38.8±11.8 μm and MDA-MB-231_NC migrated 24.9±9.4 μm for 4 h, respectively. Migration distance was decreased by vimentin knockdown in both cell lines and the rate of decrease was slightly greater in MCF10A cells.

Effects of vimentin knockdown on protrusion dynamics. Cell migration is governed by spatially and temporally coordinated changes in the F-actin cytoskeleton. The first step in cell migration is the generation of cell protrusions, which are plasma membranes that expand in the direction of migration. There are four types of protrusions: Lamellipodia, filopodia, blebs and invadopodia (28). Each of these protrusions uniquely

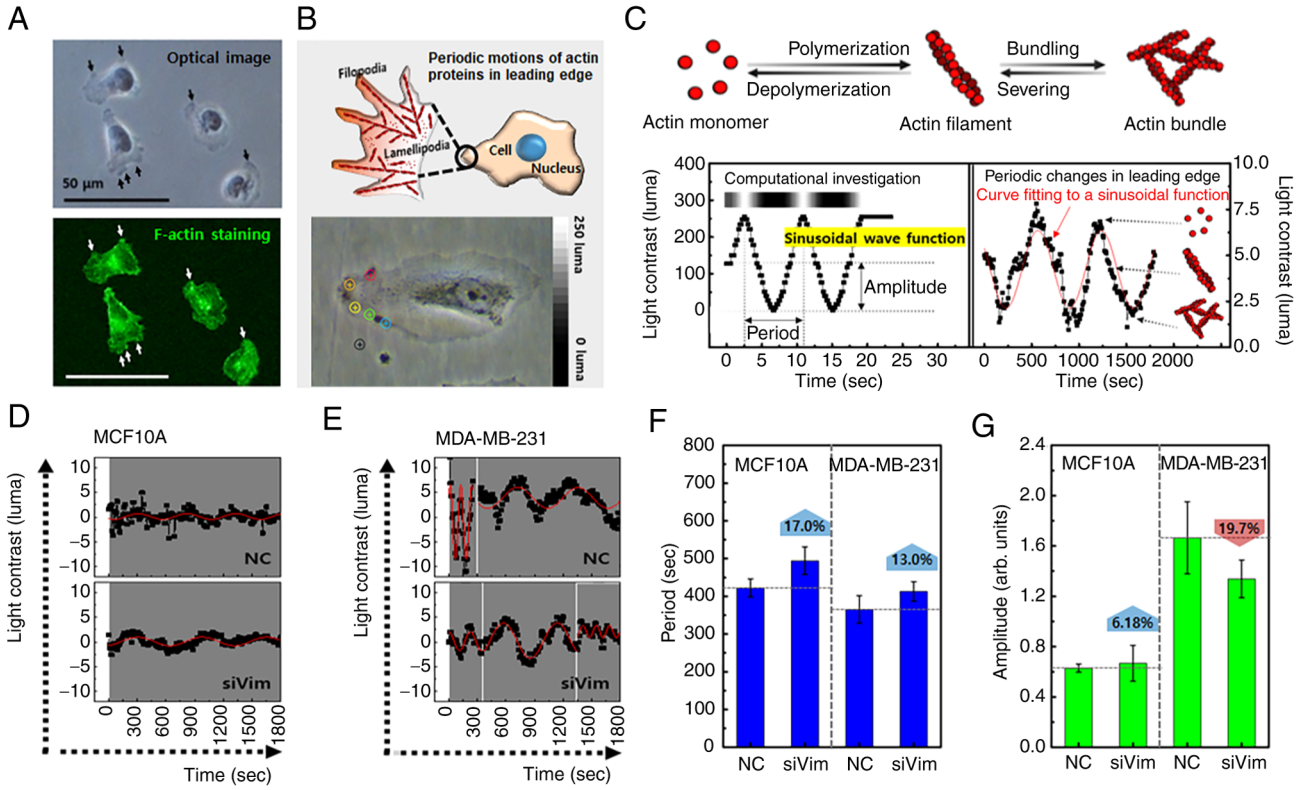

Figure 4. Altered parodic mobility of cells due to vimentin knockdown. (A) Optical and fluorescence imaging of cells showing F-actin distribution. (B) Protrusion movement along the membrane edge was observed in real-time. (C) Dynamics of protrusion were observed by the brightness change of the optical image and then converted into a numerical value (luma). Brightness changes of protrusions as a function of time were analyzed in (D) MCF10A and (E) MDA-MB-231 cells. The red line represents the curve fit to the sinusoidal function and the white line indicates the change in the period of light contrast, respectively. (F) Period and (G) amplitude were analyzed in the brightness changes of protrusion. P>0.05 in both cells. si, small interfering; NC, negative control.

contributes to migration, depending on specific circumstances, such as the cell type and microenvironment.

The present study quantitatively analyzed the effects of vimentin knockdown on protrusion dynamics using an optical microscope. First, it was confirmed that the change in brightness of the protrusion observed with a real-time optical microscope was consistent with the fluorescence distribution of F-actin (Fig. 4A). F-actin was concentrated in the dark region of the continuously moving protrusions. Therefore, moving protrusions along the membrane edge were selected for the real-time analysis (Fig. 4B). The protrusions were dynamic. For example, cells expand their lamellipodia for 100-400 sec after external stimulation and then contract (29). Cells were imaged at 10 sec intervals for 30 min and a total of 180 frames were recorded. Using an image analysis program, the brightness change in the optical image was converted into a numerical value (luma) (Fig. 4C). Luma was defined as the relative luminance and showed the level of brightness in an image. Black in the image corresponded to 0 luma and white corresponded to 250 luma. Areas with high accumulation of cytoskeletal and cytoplasmic proteins appear dark and areas with low accumulation appear bright. The F-actin appeared dark because it was relatively dense compared with that of G-actin. Thus, a luma close to 0 and 250 indicated more F- and G-actin, respectively. If the polymerization and depolymerization of F-actin occurred periodically, the change in image brightness could be expressed as a periodic function (Fig. S3). In the periodic function, the period represents the rate of actin polymerization/depolymerization and the amplitude indicates the content of F-actin or G-actin. Fig. 4D illustrates the variations in protrusion brightness as a function of time in MCF10A cells. This was not perfect however; the brightness varied periodically (Fig. S3). The brightness changes in MDA-MB-231 cells showed more periodic behavior with a larger amplitude (Fig. 4E). The period of MCF10A cells was longer than that of MDA-MB-231 cells and was slightly increased by vimentin knockdown in both cell lines (Fig. 4F). The amplitude of MDA-MB-231_NC was 2.5 times larger than that of MCF10A_NC and was decreased by vimentin knockdown (Fig. 4G).

These results indicated that the reduction in vimentin affected the formation of protrusions and their mobility in MDA-MB-231 cells. Protrusions are regulated by the relationship between the intracellular F-actin and matrix (30). If the F-actin is coupled to the matrix, newly polymerized F-actin can be converted into a protrusion. However, even if F-actin was polymerized at the leading edge of the cells, protrusions could not form if the F-actin was not attached to the matrix. As shown in Fig. 3F, protrusions developed in all directions in the MDA-MB-231_siVim cells, indicating that vimentin knockdown accelerated the formation of protrusions. This change could be related to the promotion of actin polymerization and integrin β_1 expression after vimentin knockdown, as shown in Fig. 2D and E. However, the formation rate and size of each

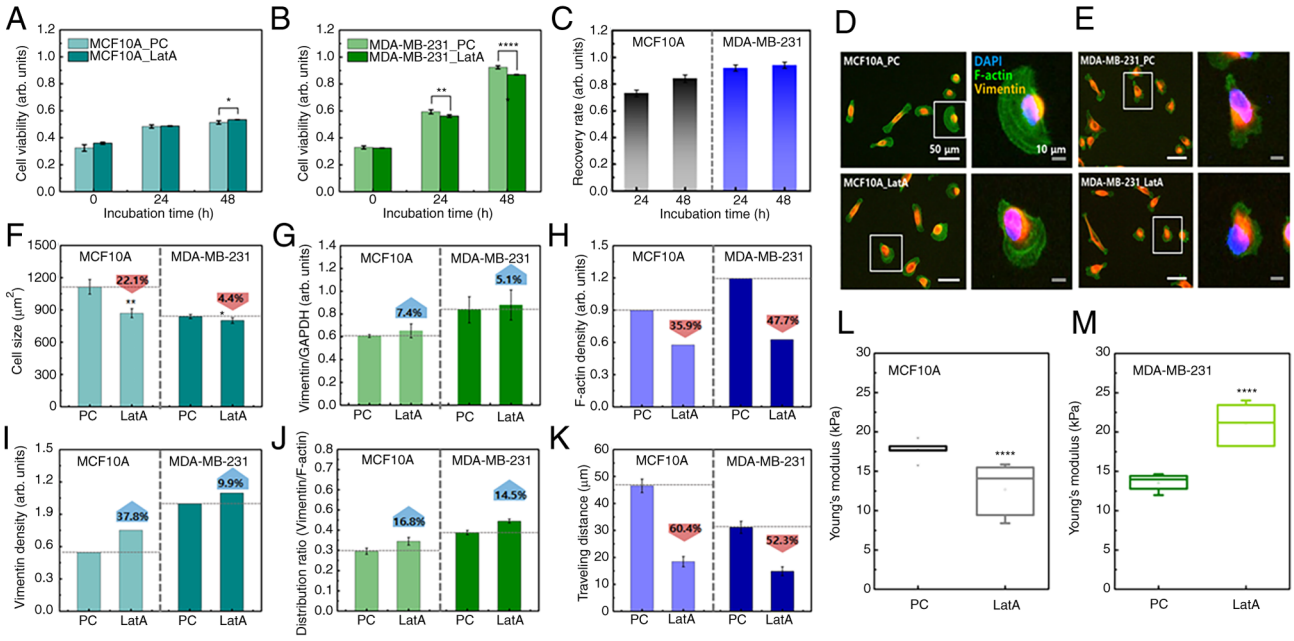

Figure 5. Comparison of cell viability between PC and F-actin depolymerized cells, (A) MCF10A and (B) MDA-MB-231. (C) Recovery of cell viability after 24 and 48 h of LatA treatment. Recovery of MCF10A and MDA-MB-231 cells was calculated from cell viability in (A) and (B), respectively. Immunofluorescence staining of vimentin and F-actin in (D) MCF10A_LatA and (E) MDA-MB-231_LatA cells. Changes in (F) cell size and (G) vimentin contents by F-actin depolymerization. (H) The F-actin density of MCF10A and MDA231 cells was calculated from cell size (F) and F-actin content, which was reduced by 53% with LatA 0.5 μM and LatA 0.3 μM, respectively (Fig. S4B). (I) Vimentin density was calculated from cell size (F) and vimentin contents (G). (J) The distribution ratio of F-actin and vimentin was calculated from the fluorescence images shown in (D) and (E). (K) Comparison of traveling distance before and after LatA treatment. Changes in Young's modulus by LatA treatment in (L) MCF10A and (M) MDA-MB-231 cells. Error bars indicate the mean ± SD (t-test). *P<0.05; **P<0.01, ****P<0.0001 vs. NC. PC, positive control; NC, negative control.

protrusion decreased in MDA-MB-231_siVim cells, which was consistent with the reduced mobility shown in Fig. 3I.

Different responses to F-actin depolymerization between cancer and normal cells. Based on the results of the vimentin-deficiency experiment, it was hypothesized that the response to F-actin reduction could differ between cancer cells and normal cells. To test these hypotheses, F-actin content was reduced by 53% following LatA treatment in both cell lines (Fig. S4) LatA-treated MCF10A cells did not show a significant change in viability compared with the positive control (PC) during long-term culture (48 h), whereas the viability of LatA-treated MDA-MB-231 cells was lower than that of the control group (Fig. 5A and B). Notably, PC indicated untreated cells. After 48 h of incubation, the recovery rates of MCF10A and MDA-MB-231 were 0.84 and 0.94, respectively (Fig. 5C). This was a relatively high recovery rate compared with that of vimentin-deficient cells, indicating that the decrease in F-actin did not significantly affect the survival of either cell. No significant change was observed in the distribution of vimentin in LatA-treated cells (Fig. 5D and E). MCF10A and MDA-MB-231 cells both shrank rapidly after LatA treatment but recovered within 4 h. Compared with the control, the cell size of MCF10A_LatA decreased by 22.1%, whereas that of MDA-MB-231_LatA slightly decreased by 4.4% (Fig. 5F). Vimentin content increased slightly in both LatA-treated cell lines, but the increase was not statistically significant (Fig. 5G). Following the LatA treatment, the average F-actin content was divided by the mean cell size. The F-actin density decreased in both cell lines. However, this reduction was more pronounced in the MDA-MB-231 cells (Fig. 5H). This notable decrease in the number of MDA-MB-231 cells could be related to a small change in cell size, as shown in Fig. 5F. The density of vimentin increased by 37.8 and 9.9% in the LatA-treated MCF10A and MDA-MB-231 cells, respectively (Fig. 5I). The intracellular distribution range of vimentin, compared with that of F-actin in both cell types after F-actin depolymerization, increased by 16.8 and 14.5% in LatA-treated MCF10A and MDA-MB-231 cells, respectively (Fig. 5J). These results indicated that there was no compensation for F-actin reduction in either cell type. The migration distance was reduced by F-actin depolymerization in both cell lines (Fig. 5K). In MCF10A, the distance traveled over 4 h decreased from 46.5±2.5 μm to 18.4±1.9 μm due to reduced F-actin. The traveling distance was decreased from 31.1±2.2 μm to 14.8±1.6 μm in MDA-MB-231. As F-actin was the most essential component of cell migration, this result was predictable. The change in cellular elasticity due to the decrease in F-actin showed opposite results to those caused by vimentin deficiency. The Young's modulus of MCF10A cells decreased by 34.6% owing to F-actin reduction, whereas that of MDA-MB-231 cells increased by 36.9% (Fig. 5L and M and S5).

Decrease in the recovery rate and motility due to simultaneous deficiency of F-actin and vimentin. The simultaneous depletion of vimentin and F-actin significantly impaired cell growth and motility. Upon simultaneous depletion of both cytoskeletal proteins, the viability of MCF10A cells remained similar until 24 h and then decreased at 48 h (Fig. 6A). MDA-MB-231 cells proliferated slightly even after simultaneous depletion of

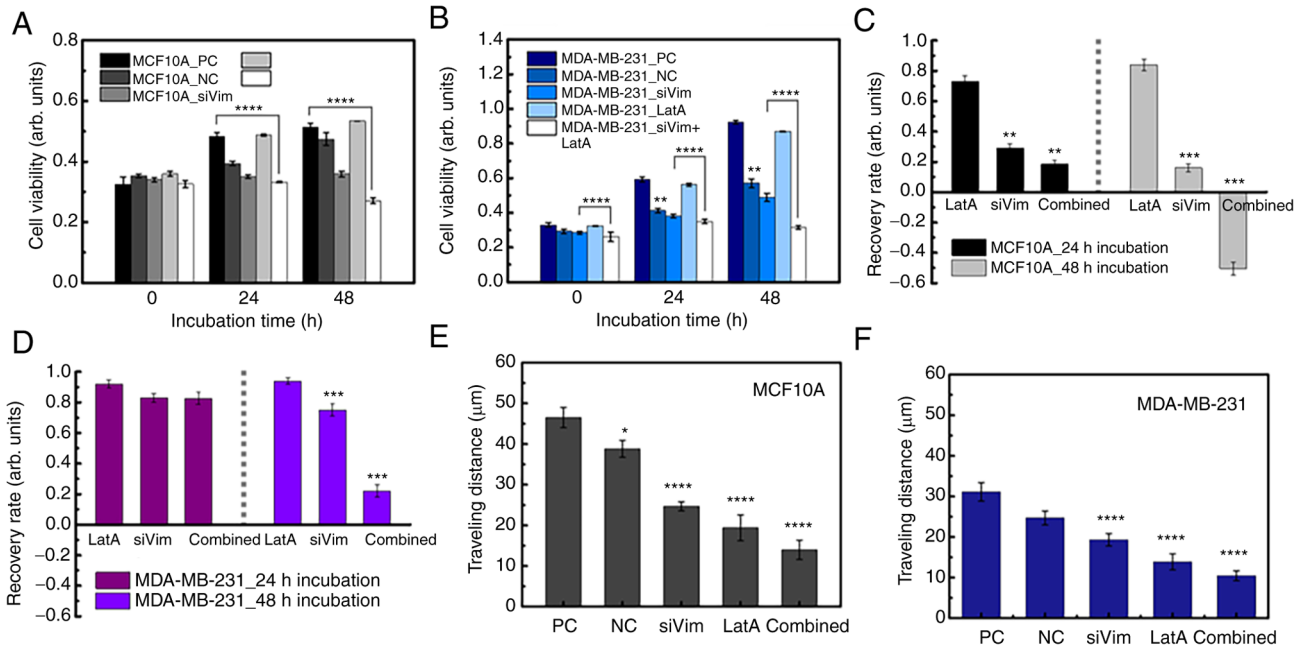

Figure 6. Comparing the effects of vimentin and F-actin deficiency on MCF10A and MDA-MB-231. Effects of simultaneous depletion of vimentin and F-actin on cell viability in (A) MCF10A and (B) MDA-MB-231 cells. Comparison of cell viability recovery following the treatment conditions of (C) MCF10A and (D) MDA-MB-231 cells. The recovery of MCF10A and MDA-MB-231 cells was calculated from Fig. 6A and B, respectively. Comparison of migration ability following the treatment conditions of (E) MCF10A and (F) MDA-MB-231 cells. The one-way ANOVA was performed on all groups and if significant differences were observed (P<0.05), post hoc analysis using Tukey's test was performed. The significant differences were indicated based on the reference groups, PC (A, B, E and F) or Lat A (C and D), highlighting the groups that exhibited significant variations. *P<0.05, **P<0.01, ***P<0.001, ****P<0.0001 vs. PC, positive control; NC, negative control; si, small interfering.

vimentin and F-actin (Fig. 6B). At 24 and 48 h, the viability of the MDA-MB-231 cells was higher than that at 0 h. The recovery rates of both normal and cancer cells according to the depletion conditions of cytoskeletal proteins were interesting. The viability of normal cells was not significantly affected by F-actin reduction and gradually restored over time; however, viability did not recover when vimentin was disrupted (Fig. 6C). Cell death occurred 48 h after the disruption of both vimentin and F-actin. In the case of MDA-MB-231 cells, when F-actin or vimentin was partially depleted separately, the survival rate was hardly affected and the cells grew to a level similar to that of the control group (Fig. 6D). Although MDA-MA-213 cells grew even after simultaneous depletion of the two proteins, cell growth was significantly inhibited compared with that in the PC and NC groups. To evaluate which condition had the most significant effect on cell migration, traveling distance was measured in cells treated with different conditions of PC, LatA treatment and combined treatment (siVim+LatA), separately. For comparison in all cases, the traveling distances of NC and siVim cells were taken from Fig. 3I. The migratory ability of both MCF10A and MDA-MB-231 cells was significantly reduced by the simultaneous deletion of vimentin and F-actin (Fig. 6E and F). F-actin depletion also had a significant effect on the mobility of both cell types. The effect of vimentin depletion on cell mobility was greater in MCF10A cells than in MDA-MB-213 cells (Table SI).

Discussion

Metastasis and therapeutic resistance are major problems in breast cancer (25-29). The present study investigated the effect of vimentin and F-actin deficiency on the survival and function of metastatic breast cancer cells and discovered some intriguing results (Fig. 7A).

In breast cancer cells, F-actin compensates for vimentin deficiency. Vimentin is highly expressed in breast, prostate, lung and malignant melanoma cancers (12). The upregulation of vimentin is associated with poor prognosis (8,9). Vimentin serves an important role in cancer metastasis by mediating the maturation of focal adhesions and the reorganization of cytoskeletal structures to maintain mechanical integrity during EMT (31). When the amount of vimentin in breast cancer cells was decreased by 57%, the amount of F-actin increased by ~21%. The amount of integrin β_1 and the cell size also increased by 29 and 14%, respectively. This indicated that actin polymerization is promoted to compensate for the decrease in vimentin expression, leading to the expression of integrins that link intracellular F-actin to the substrate, resulting in improved cell adhesion to the substrate. In normal cells, the expression of F-actin and integrin β_1 decreases with a decrease in vimentin expression, leading to a decrease in cell size. It is possible that the simultaneous decrease in vimentin and F-actin levels impairs the ability of the cell to maintain its structure and attach to the substrate.

Integrins are transmembrane proteins that connect the extracellular matrix to the cytoskeleton. Integrins bind to ligands in the extracellular matrix (ECM), such as fibronectin, vitronectin, collagen and laminin and the ligands to which an integrin can bind are determined by which α (integrin α) and β (integrin β) subunits the integrin is composed of (32). Integrin β is primarily responsible for forming focal adhesions on adherent cells and positioning integrin heterodimers in the proper location on the cell. Primarily, integrin β_1 subunit predominantly bind to

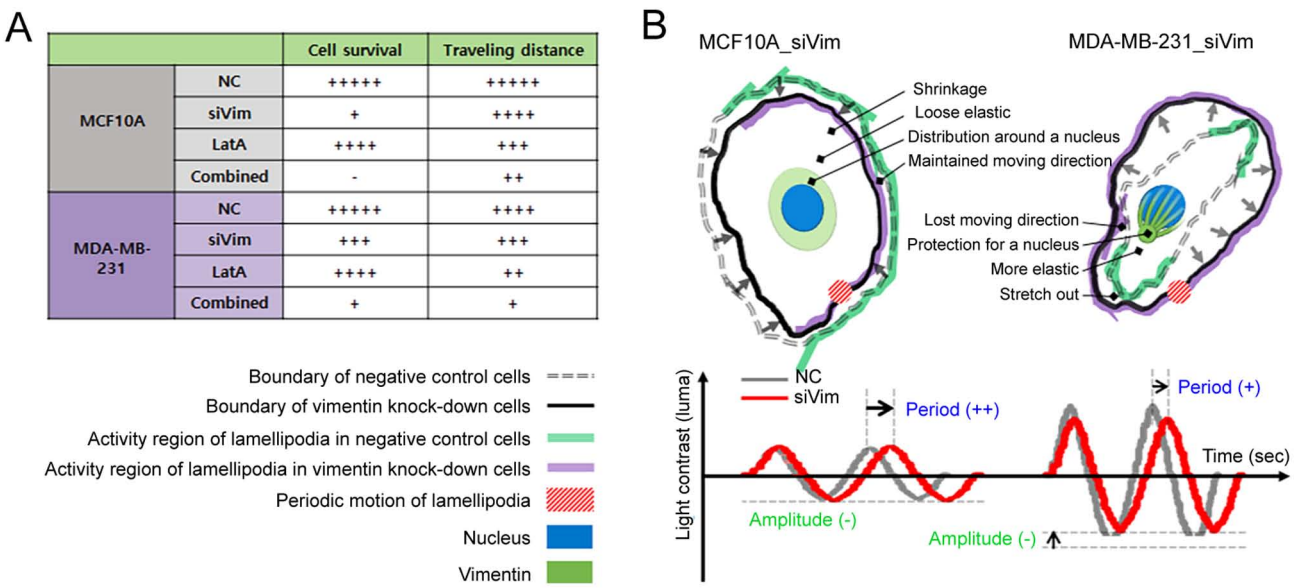

Figure 7. Summary of the effects of cytoskeletal protein deficiency on MCF10A and MDA-MB-231. (A) Cancer cells and normal cells showed different responses on cell survival and migration to reducing vimentin or F-actin, respectively. Cell survival and traveling distance values were relatively marked by the number of + or -symbols. In comparing cell recovery rate and cell mobility, the more +, the greater the cell activity. Moreover, only for the case of cell recovery rate, -means that the appearance of cell apoptosis. (B) The reduction of vimentin caused morphological changes and reorganization of F-actin and vimentin. The protrusion dynamics were also affected by vimentin deficiency.

tumor-upregulated ECM ligands, such as fibronectin, collagen I and tenascin-C (33). Thus, integrin β_1 contributes to the stability of adhesion between cells and the ECM of the tumor and facilitates cell migration via a reciprocal signaling system with F-actin. The cytoplasmic domain of integrin β_1 binds to F-actin. In breast cancer cells, the multiple downstream signaling pathways of β_1, including FAK, PI3K and ERK/MAPK, coordinating signaling through receptor tyrosine kinases, are involved in the modulation of tumor initiation, progression and ultimately metastasis (26). FAK acts as a scaffolding protein by interacting with SH3 domain-containing proteins, including p130Cas and endophilin A2 (34). In particular, its interaction with p130Cas has been demonstrated to be important in regulating cell migration and breast cancer progression (35). FAK autophosphorylation at tyrosine 397 and PI3K activation inhibits apoptosis of cells by activating Akt kinase (36,37). FAK is also involved in cell cycle regulation by forming FAK/Src complexes at focal contacts, which activate ERK and cyclin D1 but inhibit p21 expression (38). In the present study, F-actin content was manipulated, so to understand the altered motility of cancer cells, changes in the content of integrins were identified based on F-actin content. Thus, it appears that the increased expression of integrins due to a decrease in vimentin contributes to stable cell adhesion, which quickly restores cell viability in breast cancer cells.

When the F-actin content was reduced by 57% in both normal and cancer cells, the amount of vimentin increased slightly to 7.4 and 5.1% in MCF10A and MDA-MB-213 cells, respectively. The reduction in F-actin levels did not significantly impair the survival of either cell type. The size of the normal cells decreased by 27%, but the size of the cancer cells did not change significantly. As aforementioned, the relative proportion of F-actin is lower in cancer cells than in normal cells because the amount of vimentin increases during malignant transformation, whereas the amount of F-actin decreases (39,40). Therefore, a reduction in F-actin levels in cancer cells is not thought to have a significant effect on cell morphology (Fig. 7B). However, the migration distance was substantially reduced in both cell types by >50%. As aforementioned, cells migrate through actin successive polymerization and depolymerization. Therefore, the decrease in migration distance can be easily understood as the inhibition of mobility due to F-actin reduction. These results suggested that actin-targeted therapies are not very effective at killing cancer cells but are very effective at inhibiting the motility of metastatic cancer cells. Thus, combining toxic drugs with high selectivity for cancer cells with actin-targeted therapies may synergistically affect metastatic cancer cells.

While the elasticity of normal cells depends on F-actin density, the elasticity of cancer cells appears to depend primarily on vimentin density. Cancer cells are less elastic than normal cells. This was associated with reduced F-actin levels during malignant transformation. Some studies have shown that low elasticity is advantageous for cancer migration (41-45). However, conflicting results have been reported in which cells with high elasticity migrate more readily (46). The correlation between cellular elasticity and migration remains controversial; however, it is clear that lower elasticity favors invasion. To metastasize, cancer cells change their elasticity through morphological and phenotypic conversions and then detach from the primary tissues (47). Cells that have acquired motility enter lymphatic vessels or bloodstream and are seeded into distant organs. If the cellular elasticity is low, the cell can easily deform. Therefore, the low elasticity of cancer cells is advantageous for invasion. Cellular elasticity is regulated by F-actin. When the content of F-actin is high or its network is dense and well-organized, the elasticity of the cells increases. The elasticity of MCF10A and MDA-MB-231 cells is altered by vimentin knockdown and F-actin

depolymerization. However, this change was not related to F-actin content. As the cell size also changed due to the decrease in vimentin and F-actin content, the elasticity was compared with the density of the two filaments. Notably, the elastic change in MCF10A cells coincided with the change in F-actin density, whereas the elastic change in MDA-MB-231 cells followed a change in vimentin density. Based on these results, it was hypothesized that F-actin could serve a major role in the elasticity of normal cells and that vimentin could serve a key role in cancer cells.

In summary, reduction in vimentin or F-actin levels did not substantially affect the growth or migration of breast cancer cells. However, the simultaneous depletion of F-actin and vimentin had a more notable effect on the survival and motility of breast cancer cells. The cytoskeleton is considered the backbone of a cell, as it provides the cell with its shape and structure and facilitates cellular movements. The three cytoskeletal proteins-actin filaments, intermediate filaments and microtubules-have unique roles and share functions as skeletal organelles. To date, most cytoskeleton-targeting drugs developed typically target a single protein. The results of the present study showed that drugs targeting metastatic cancer cells are effective in simultaneously reducing vimentin and F-actin levels.

Acknowledgements

Not applicable.

Funding

The present study was supported by the National Research Foundation of Korea (grant no. 2021R1I1A1A01055772) funded by the Korean government (MSIT).

Availability of data and materials

The datasets used and/or analyzed in the current study are available from the corresponding author upon reasonable request.

Authors' contributions

SK and KK conceived the study and prepared the first draft of the manuscript. SK and SH conducted the experiments and analyzed the data. SK and SH critically reviewed and revised the manuscript. SK and KK confirm the authenticity of all the raw data. All authors read and approved the final manuscript.

Ethics approval and consent to participate

Not applicable.

Patient consent for publication

Not applicable.

Competing interests

The authors declare that they have no competing interests.

References

1. Lin Z, Han Y, Wu B and Fang W: Altered cytoskeletal structures in transformed cells exhibiting obviously metastatic capabilities. Cell Res 1: 141-51, 1990.
2. Fletcher DA and Mullins RD: Cell mechanics and the cytoskeleton. Nature 463: 485-492, 2010.
3. Yamaguchi H and Condeelis J: Regulation of the actin cytoskeleton in cancer cell migration and invasion. Biochim Biophys Acta 1773: 642-652, 2007.
4. Tang DD and Gerlach BD: The roles and regulation of the actin cytoskeleton, intermediate filaments and microtubules in smooth muscle cell migration. Respir Res 18: 54, 2017.
5. Liu CY, Lin HH, Tang MJ and Wang YK: Vimentin contributes to epithelial-mesenchymal transition cancer cell mechanics by mediating cytoskeletal organization and focal adhesion maturation. Oncotarget 6: 15966-15983, 2015.
6. Sun B, Fang Y, Li Z, Chen Z and Xiang J: Role of cellular cytoskeleton in epithelial-mesenchymal transition process during cancer progression. Biomed Rep 3: 603-610, 2015.
7. Battaglia RA, Delic S, Herrmann H and Snider NT: Vimentin on the move: New developments in cell migration. F1000Res 7: 1796, 2018.
8. Wu S, Du Y, Beckford J and Alachkar H: Upregulation of the EMT marker vimentin is associated with poor clinical outcome in acute myeloid leukemia. J Transl Med 16: 170, 2108.
9. Tadokoro A, Kanaji N, Liu D, Yokomise H, Haba R, Ishii T, Takagi T, Watanabe N, Kita N, Kadowaki N and Bandoh S: Vimentin regulates invasiveness and is a poor prognostic marker in non-small cell lung cancer. Anticancer Res 36: 1545-1551, 2106.
10. Kwon S, Yang W, Moon D and Kim KS: Comparison of cancer cell elasticity by cell type. J Cancer 11: 5403-5412, 2020.
11. Li X, Kierfeld J and Lipowsky R: Actin polymerization and depolymerization coupled to cooperative hydrolysis. Phys Rev Lett 103: 048102, 2009.
12. Satelli A and Li S: Vimentin in cancer and its potential as a molecular target for cancer therapy. Cell Mol Life Sci 68: 3033-3046, 2011.
13. Peng GE, Wilson SR and Weiner OD: A pharmacological cocktail for arresting actin dynamics in living cells. Mol Biol Cell 22: 3986-3994, 2011.
14. Stehn JR, Haass NK, Bonello T, Desouza M, Kottyan G, Treutlein H, Zeng J, Nascimento PRBB, Sequeira VB, Butler TL, *et al*: A novel class of anticancer compounds targets the actin cytoskeleton in tumor cells. Cancer Res 73: 5169-5182, 2013.
15. Tang K, Xin Y, Li K, Chen X and Tan Y: Cell cytoskeleton and stiffness are mechanical indicators of organotropism in breast cancer. Biology (Basel) 10: 259, 2021.
16. Gandalovičová A, Rosel D, Fernandes M, Veselý P, Heneberg P, Čermák V, Petruželka L, Kumar S, Sanz-Moreno V and Brábek J: Migrastatics-anti-metastatic and anti-invasion drugs: Promises and challenges. Trends Cancer 3: 391-406, 2017.
17. Fife CM, McCarroll JA and Kavallaris M: Movers and shakers: Cell cytoskeleton in cancer metastasis. Brit J Pharmacol 171: 5507-5523, 2014.
18. Atteeq M: Evaluating anticancer properties of withaferin A-a potent phytochemical. Front Pharmacol 13: 975320, 2022.
19. Nagy Z, Cheung BB, Tsang W, Tan O, Herath M, Ciampa OC, Shadma F, Carter DR and Marshall GM: Withaferin A activates TRIM16 for its anti-cancer activity in melanoma. Sci Rep 10: 19724, 2020.
20. Burikhanov R, Sviripa VM, Hebbar N, Zhang W, Layton WJ, Hamza A, Zhan CG, Watt DS, Liu C and Rangnekar VM: Arylquins target vimentin to trigger Par-4 secretion for tumor cell apoptosis. Nat Chem Biol 10: 924-926, 2014.
21. Cheratta AR, Thayyullathil F, Pallichankandy S, Subburayan K, Alakkal A and Galadari S: Prostate apoptosis response-4 and tumor suppression: It's not just about apoptosis anymore. Cell Death Dis 12: 47, 2021.
22. Giganti A and Friederich E: The actin cytoskeleton as a therapeutic target: State of the art and future directions. Prog Cell Cycle Res 5: 511-525, 2003.
23. Cramer LP: Role of actin-filament disassembly in lamellipodium protrusion in motile cells revealed using the drug jasplakinolide. Curr Biol 9: 1095-1105, 1999.
24. Strouhalova K, Přechová M, Gandalovičová A, Brábek J, Gregor M and Rosel D: Vimentin intermediate filaments as potential target for cancer treatment. Cancers (Basel) 12: 184, 2020.

25. Han R and Chen J: A modified Sneddon model for the contact between conical indenters and spherical samples. J Mater Res 36: 1762-1771, 2021.
26. Hou S, Isaji T, Hang Q, Im S, Fukada T and Gu J: Distinct effects of integrin β_1 on cell proliferation and cellular signaling in MDA-MB-231 breast cancer cells. Sci Rep 6: 18430, 2016.
27. Vinckier A and Semenza G: Measuring elasticity of biological materials by atomic force microscopy. FEBS Lett 430: 12-16, 1998.
28. Ridley AJ: Life at the leading edge. Cell 145: 1012-1022, 2011.
29. Gagliardi PA, Puliafito A, Blasio L, Chianale F, Somale D, Seano G, Bussolino F and Primo L: Real-time monitoring of cell protrusion dynamics by impedance responses. Sci Rep 5: 10206, 2015.
30. Wilson K, Lewalle A, Fritzsche M, Thorogate R, Duke T and Charras G: Mechanisms of leading-edge protrusion in interstitial migration. Nat Commun 4: 2896, 2013.
31. Duarte S, Viedma-Poyatos Á, Navarro-Carrasco E, Martínez AE, Pajares MA and Pérez-Sala D: Vimentin filaments interact with the actin cortex in mitosis allowing normal cell division. Nat Commun 10: 4200, 2019.
32. Mezu-Ndubuisi OJ and Maheshwari A: The role of integrins in inflammation and angiogenesis. Pediatr Res 89: 1619-1626, 2021.
33. Alberts B, Johnson A, Lewis J, Raff M, Roberts K and Walter P: Molecular biology of the cell. 4th edition. New York: Garland Science, 2002.
34. Luo M and Guan JL: Focal adhesion kinase: A prominent determinant in breast cancer initiation, progression and metastasis. Cancer Lett 289: 127-139, 2010.
35. Gemperle J, Dibus M, Koudelková L, Rosel D and Brábek J: The interaction of p130Cas with PKN3 promotes malignant growth. Mol Oncol 13: 264-289, 2019.
36. Madan R, Smolkin MB, Cocker R, Fayyad R and Oktay MH: Focal adhesion proteins as markers of malignant transformation and prognostic indicators in breast carcinoma. Hum Pathol 37: 9-15, 2006.
37. Guan JL and Shalloway D: Regulation of focal adhesion-associated protein tyrosine kinase by both cellular adhesion and oncogenic transformation. Nature 358: 690-692, 1992.
38. Guan JL: Integrin signaling through FAK in the regulation of mammary stem cells and breast cancer. IUBMB Life 62: 268-276, 2010.
39. Hahm ER, Mathan SV, Singh RP and Singh SV: Breast cancer selective disruption of actin cytoskeleton by diallyl trisulfide. J Cancer Prev 27: 101-111, 2022.
40. Meng Z, Li Z, Xie M, Yu H, Jiang L and Yao X: TM9SF4 is an F-actin disassembly factor that promotes tumor progression and metastasis. Nat Commun 13: 5728, 2022.
41. Mierke CT: Mechanical cues affect migration and invasion of cells from three different directions. Front Cell Dev Biol 8: 583226, 2020.
42. Jonietz E: Mechanics: The forces of cancer. Nature 491: S56-S57, 2012.
43. Alibert C, Goud B and Manneville JB: Are cancer cells really softer than normal cells? Biol Cell 109: 167-189, 2017.
44. Xu W, Mezencev R, Kim B, Wang L, McDonald J and Sulchek T: Cell stiffness is a biomarker of the metastatic potential of ovarian cancer cells. PLoS One 7: e46609, 2012.
45. Kim TH, Gill NK, Nyberg KD, Nguyen AV, Hohlbauch SV, Geisse NA, Nowell CJ, Sloan EK and Rowat AC: Cancer cells become less deformable and more invasive with activation of β-adrenergic signaling. J Cell Sci 129: 4563-4575, 2016.
46. Sahai E: Illuminating the metastatic process. Nat Rev Cancer 7: 737-749, 2007.
47. Pachmayr E, Treese C and Stein U: Underlying mechanisms for distant metastasis-molecular biology. Visc Med 33: 11-20, 2017.